Heat Capacity and Thermodynamic Functions of Sodium Rare Earth Ternary Fluorides

Alexis Gibson

A senior thesis submitted to the faculty of

Brigham Young University

In partial fulfillment of the requirements for the degree of

Bachelor of Science

Brian Woodfield, Research Advisor

Branton Campbell, Department Advisor

Department of Physics and Astronomy

Brigham Young University

April 2022

ABSTRACT

Heat Capacity and Thermodynamic Functions of Sodium Rare Earth Ternary Fluorides

Alexis Gibson

Department of Physics and Astronomy, BYU

Bachelor of Science

Sodium rare earth ternary fluorides, $NaREF_4$ (RE = rare earth), are an important class of materials because they are intermediate compositions for rare earth element extraction and can act as up-conversion phosphors. To better understand their physical properties, energetics, and stability, we measured the heat capacity of three β-structured $NaREF_4$ compounds, $NaNdF_4$, $NaYbF_4$, and $NaYF_4$, from 1.8 K to 300 K. Our measurements show an upturn in the low temperature heat capacity of each sample, which we attribute to the splitting of degenerate nuclear magnetic states. We provide calculations of the effective field causing the splitting for each sample. We also report standard entropy, standard enthalpy, and Gibbs free energy at selected temperatures from 0 to 300 K.

Keywords: Heat capacity; Schottky anomaly; Hyperfine field splitting; Rare earth; Ternary fluoride

ACKNOWLEDGEMENTS

I would like to thank Dr. Woodfield for his guidance, instruction, and patience. I would also like to thank the BYU College of Physical and Mathematical Sciences for giving me the resources required to reach this point. Finally, I would like to thank my family for their constant support.

List of Figures

Figure 1: PXRD patterns of $Na_{1.5}RE_{1.5}F_6$ samples 8

Figure 2: Plot of Molar Heat Capacity Data 12

Figure 3: Plot of Low Temperature Molar Heat Capacity Data 13

Figure 4: Low Temperature Fit Deviation Plot 14

Figure 5: Mid Temperature Fit Deviation Plot 15

Figure 4: High Temperature Fit Deviation Plot 17

List of Tables

Table 1: Measurement Details 10

Table 2: Fitting Parameters 18

Table 3: $NaNdF_4$ Measured Molar Heat Capacity 21

Table 4: $NaYbF_4$ Measured Molar Heat Capacity 22

Table 5: $NaYF_4$ Measured Molar Heat Capacity 23

Table 6: $NaNdF_4$ Standard Thermodynamic Functions 24

Table 7: $NaYbF_4$ Standard Thermodynamic Functions 25

Table 8: $NaYF_4$ Standard Thermodynamic Functions 26

Table of Contents

LIST OF FIGURES....4

LIST OF TABLES....4

TABLE OF CONTENTS....5

CHAPTER 1: INTRODUCTION....6

1.1 Sodium Rare Earth Ternary Fluorides.... 6

1.2 Heat Capacity Overview.... 6

CHAPTER 2: EXPERIMENTAL METHODS....8

2.1 Sample Preparation and Characterization.... 8

2.2 PPMS and Thermal Relaxation Calorimetry.... 8

2.3 Heat Capacity Measurement Procedure.... 9

2.4 Fitting Regions Overview.... 10

CHAPTER 3: RESULTS AND DISCUSSION....12

3.1 Collected Data.... 12

3.2 Low Temperature Region Curve Fitting.... 13

3.3 Middle Temperature Region Curve Fitting.... 15

3.4 High Temperature Region Curve Fitting.... 16

3.5 Low Temperature Upturns.... 19

3.6 Hyperfine Field Calculations.... 20

3.7 Conclusions.... 20

APPENDIX....21

BIBLIOGRAPHY....27

INDEX....30

Contents of this thesis will be submitted for publication May 2022

Chapter 1: Introduction

1.1 Sodium Rare Earth Ternary Fluorides

Sodium rare earth ternary fluorides, $NaREF_4$, have valuable photoluminescent properties with important technical applications in medicine and technology [1-5]. Several studies have explored the effects of synthesis and doping techniques on material attributes such as particle size, structure, and luminescent properties [1-3, 5-7].

Despite the importance of chemical thermodynamics in understanding function and stability, few studies have explored the thermodynamics of these materials [4, 8-10]. Yang, Anderko [8] recently determined the heats of formation of several $NaREF_4$, but their heat capacity, and consequently the absolute entropy of these materials, remain unmeasured.

In this work, we measured the heat capacity of three $NaREF_4$ samples, $NaNdF_4$, $NaYbF_4$, and $NaYF_4$, from 1.8 K to 300 K. Models fitted to heat capacity data were used to generate standard thermodynamic functions, assess stability, and calculate hyperfine field values for rare earth nuclei.

1.2 Heat Capacity Overview

The field of chemical thermodynamics is a theoretical framework used to study macroscopic systems consisting of a very large number of microscopic components. In a system at constant pressure with no chemical reactions taking place, heat transfer is equivalent to a change in enthalpy. In this case, the first law of thermodynamics can be written as:

$$dU = dH - PdV \tag{1.1}$$

where *U* is the internal energy, *P* is Pressure, *V* is volume, and *H* is the enthalpy.

The heat capacity of the system, the change in energy per change in temperature, takes two forms [11, 12] :

$$C_p = \left(\frac{dH}{dT}\right)_p \text{ and } C_V = \left(\frac{dU}{dT}\right)_V \tag{1.2}$$

In this notation, the subscript indicates which variable is being held constant.

A material's heat capacity is one of its most fundamental properties and gives valuable engineering and thermodynamic insight. It is possible to model heat capacity data with smoothed functions; however, making use of theoretical models that account for different energy mode contributions (e.g., lattice, magnetic, electronic) is preferred. Fitting with these theoretical functions gives the researcher more insight into material properties.

Thermodynamic functions, including entropy ($S_\mathrm{m}°$), enthalpy ($H_\mathrm{m}°$), and Gibbs free energy ($G_\mathrm{m}°$), are calculated according to the following relations:

$$\Delta_0^T S_\mathrm{m}° = \int_0^T \frac{C_{p,\mathrm{m}}(T)}{T}\, dT \tag{1.3}$$

$$\Delta_0^T H_\mathrm{m}° = \int_0^T C_{p,\mathrm{m}}(T)\, dT \tag{1.4}$$

$$\Delta_0^T G_\mathrm{m}° = \Delta_0^T H_\mathrm{m}° - T\, \Delta_0^T S_\mathrm{m}° \tag{1.5}$$

It is common to remove most of the temperature dependence of the Gibbs free energy function by dividing by *T*. Doing this allows for easier extrapolation at smoothed temperature intervals. The result, $\Phi_\mathrm{m}°$, is reported at smoothed temperatures along with $\Delta_0^T S_\mathrm{m}°$ and $\Delta_0^T H_\mathrm{m}°$.

Chapter 2: Experimental Methods

2.1 Sample Preparation and Characterization

Samples were prepared using solid state reactions between NaF and rare earth trifluorides (REF_3). Samples were then characterized using powder X-ray diffraction (PXRD). PXRD patterns used to confirm composition and phase purity are shown in Figure 2.1. Full synthesis and characterization details for these samples have been reported by Yang et al. [8].

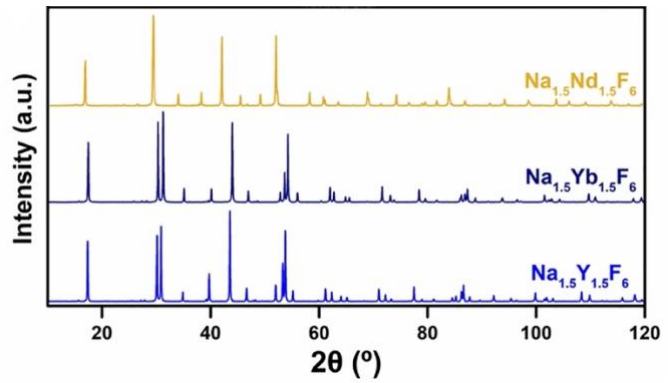

Figure 1: PXRD spectra of $Na_{1.5}RE_{1.5}F_6$. Adapted from Yang et al. [8].

2.2 PPMS and Thermal Relaxation Calorimetry

The Quantum Design Physical Property Measurement System (PPMS) is a versatile laboratory apparatus capable of preforming several different measurements. The heat capacity option enables the PPMS to act as a fully automated relaxation calorimeter. Equipped with the ^{4}He cooling system, the PPMS is able to measure heat capacity between 1.8 K and 400 K [13, 14].

Like other heat capacity measurement techniques, thermal relaxation calorimetry involves adding a known amount of heat to a sample and measuring the resultant change in temperature. A weak thermal link connects the sample platform to a heat sink and a known power is applied for a designated amount of time. When heat flow ends, the sample assembly begins to cool to the heat sink's temperature. The heat capacity is calculated from the platform's temperature relaxation curve and the measured thermal conductivity obtained from the heating stage of the measurement [14-16]. Benefits of relaxation calorimetry include smaller sample size (generally 1–100 mg), faster measurement times, and reasonable accuracy and precision [13, 15, 16].

2.3 Heat Capacity Measurement Procedure

Heat capacity measurements were performed with a Quantum Design Physical Property Measurement System (PPMS) in zero magnetic field from 1.8 to 300 K. A method devised for measuring the heat capacities of insulating powders was used for sample preparation [15, 17]. Details of this method are given below.

The sample was enclosed in a copper cup (0.025 mm thick, 99.999% purity from Alfa Aesar). Two small copper coils were inserted into the cup to ensure uniform heating throughout the sample [13]. After being pressed into a pellet, the sample was attached to the sample holder using a small amount of Apiezon N grease and placed in the PPMS. Prior to measuring the sample's heat capacity, an addenda measurement was performed to account for the heat capacity of the sample platform and grease. This method has an estimated accuracy of ± 2 % below 10 K and ± 1 % from 10 to 300 K [15, 17]. The sample and copper masses used are listed in Table 1.

Table 1. Details of the PPMS calorimetric measurements including pressures (p), sample mass (m_s), and copper mass (m_{Cu}). The estimated standard uncertainties in the masses $m_{s,Cu}$ and pressure p are $u(m_{s,Cu}) = 0.06$ mg and $u(p) = 0.1$ mPa.

	p / mPa	m_s / mg	m_{Cu} / mg
$NaNdF_4$	1.2	15.724	18.000
$NaYbF_4$	1.2	14.264	16.940
$NaYF_4$	1.2	10.978	20.080

2.4 Fitting Regions Overview

The heat capacity of a material can generally be divided into three fitting regimes: low temperature ($T \lesssim 15$ K), mid temperature ($5\text{ K} \lesssim T \lesssim 65$ K), and high temperature ($T \gtrsim 40$ K). Adjacent regions are connected through an overlap point where fits intersect and have similar first and second derivatives.

The heat capacity is the sum of different contributors (e.g., lattice, electronic, and magnetic contributions). Therefore, a linear combination of theoretical functions, each representing a specific contribution, is used to model the low and high temperature regions. Initial parameters for these functions are based on physical values and material properties. A final fit is decided upon through careful examination of RMS deviation, the deviation plot, and parameter acceptability.

Several phenomena are detectable in the low temperature regime because the lattice contribution becomes less dominant [11, 13]. The present phenomena greatly depend on the material, so there is no single theoretical model that can be applied to all samples. Instead, it is beneficial to attempt fitting several combinations of possible heat capacity contributions against the data. These contributions should be compared to sample composition to determine if the fit is physically acceptable.

The high temperature region is typically fitted with a combination of Einstein and Debye functions [13]. These functions represent the contribution of lattice vibrations at higher temperatures [11]. The high temperature region can also feature first and second order phase transitions if they are present [13, 16].

Because theoretical functions rarely apply to the mid temperature region, this region is generally fitted with an orthogonal polynomial, which provides a smooth transition between the low and high temperature regions.

Chapter 3: Results and Discussion

3.1 Results

Graphs of the molar heat capacities of $NaNdF_4$, $NaYbF_4$, and $NaYF_4$, are plotted versus temperature in Figure 2 where the lines represent the fits of the data. Shown in Figure 3 is an expanded view of the heat capacity data below 10 K. Tables containing the measured experimental data are included in the appendix. The experimental heat capacity is smooth without any features except in the low temperature region below 6 K. $NaNdF_4$ and $NaYbF_4$ exhibit upturns in the data and $NaYF_4$ has a small Schottky anomaly not visible in the graph. We attribute these features to nuclear Schottky anomalies that arise from the nuclear moments of some isotopes of Nd, Yb, and Y. These upturns are discussed in more detail below.

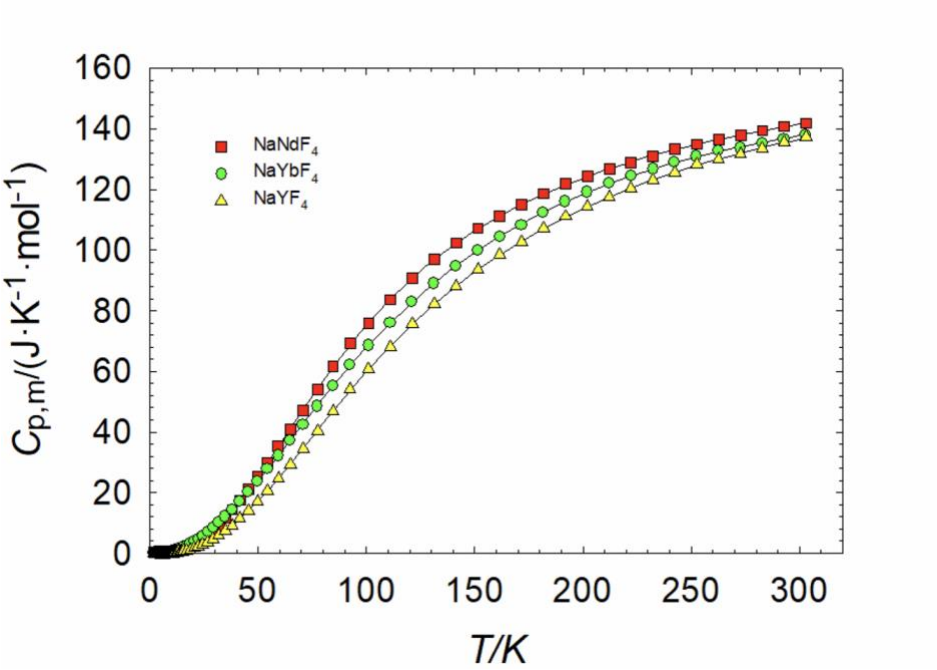

Figure 2. Plot of the molar heat capacity data for NaNdF4, NaYbF4, and NaYF4 at constant pressure. Black curves behind data are fits discussed in 3.2-3.4.

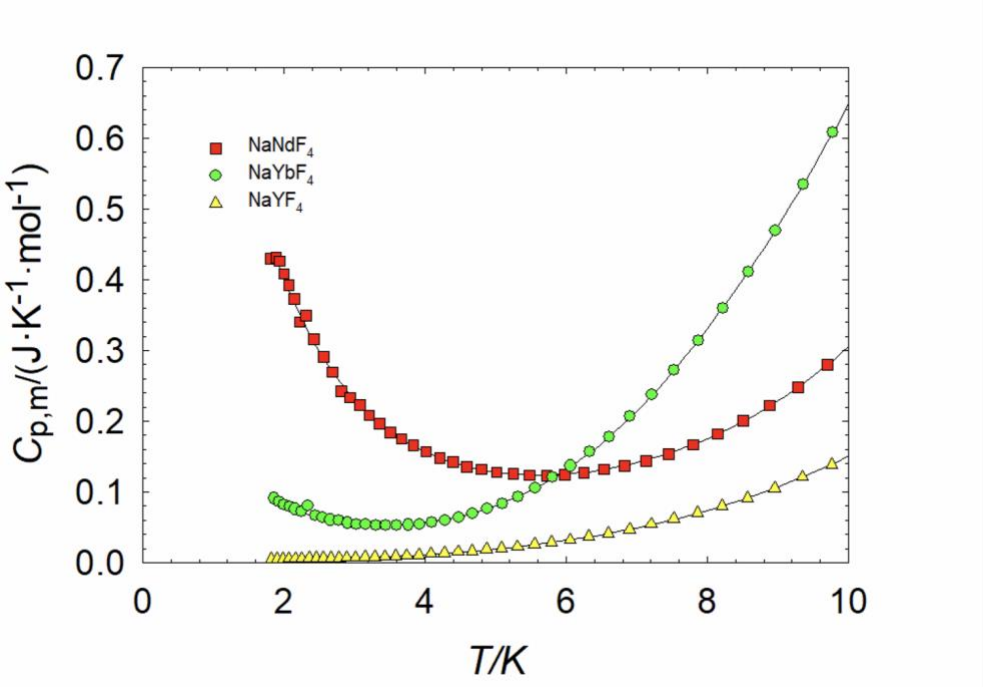

Figure 3. Plot of the low temperature (T < 10 K) molar heat capacity data for NaNdF4, NaYbF4, and NaYF4 at constant pressure. Black curves behind data are fits discussed in 3.2. Heat capacity features prominent upturns which are discussed in 3.5.

3.2 Low Temperature Region Curve Fitting

Following the procedure discussed in section 2.4, the heat capacity data below 10 K was fitted according to the function:

$$C_{p,\mathrm{m}} = B_1T^1 + B_3T^3 + B_5T^5 + B_7T^7 + C_2T^{-2} + C_3T^{-3} \quad (3.1)$$

The system's Hamiltonian relates constants C_2 and C_3 to the magnetic interaction parameter, a', and the quadrupole coupling constant, P, through the expressions [18]:

$$\frac{C_2}{R} = \frac{1}{3}(a')^2 I(I+1) + \frac{1}{45}P^2 I(I+1)(2I-1)(2I+3) \quad (3.2)$$

$$\frac{C_3}{R} = -\frac{1}{15}(a')^2 PI(I+1)(2I-1)(2I+3) \quad (3.3)$$

where R is the universal gas constant, I is the nuclear spin of each isotope, and B_1, B_3, B_5, B_7, a', and P are constants obtained from fitting the data. The B_3, B_5, and B_7 terms model the lattice

contribution to the heat capacity and account for any anharmonicity in lattice phonons [11]. In insulators, a linear (B_1) term is typically required to model lattice vacancies or other impurities [19]. The final two terms in Eq. 3.1 originate from the high temperature side of a Schottky anomaly and model the low temperature upturn in the heat capacity [18]. Fitting parameters are included in Table 2. Deviation plots for low temperature heat capacity data are shown in Figure 4. Deviations from the fit remain within 4% and decrease at higher temperatures.

Note that the heat capacity terms resulting from nuclear phenomena were not included in the calculation of thermodynamic functions to isolate chemical contributions to thermodynamics.

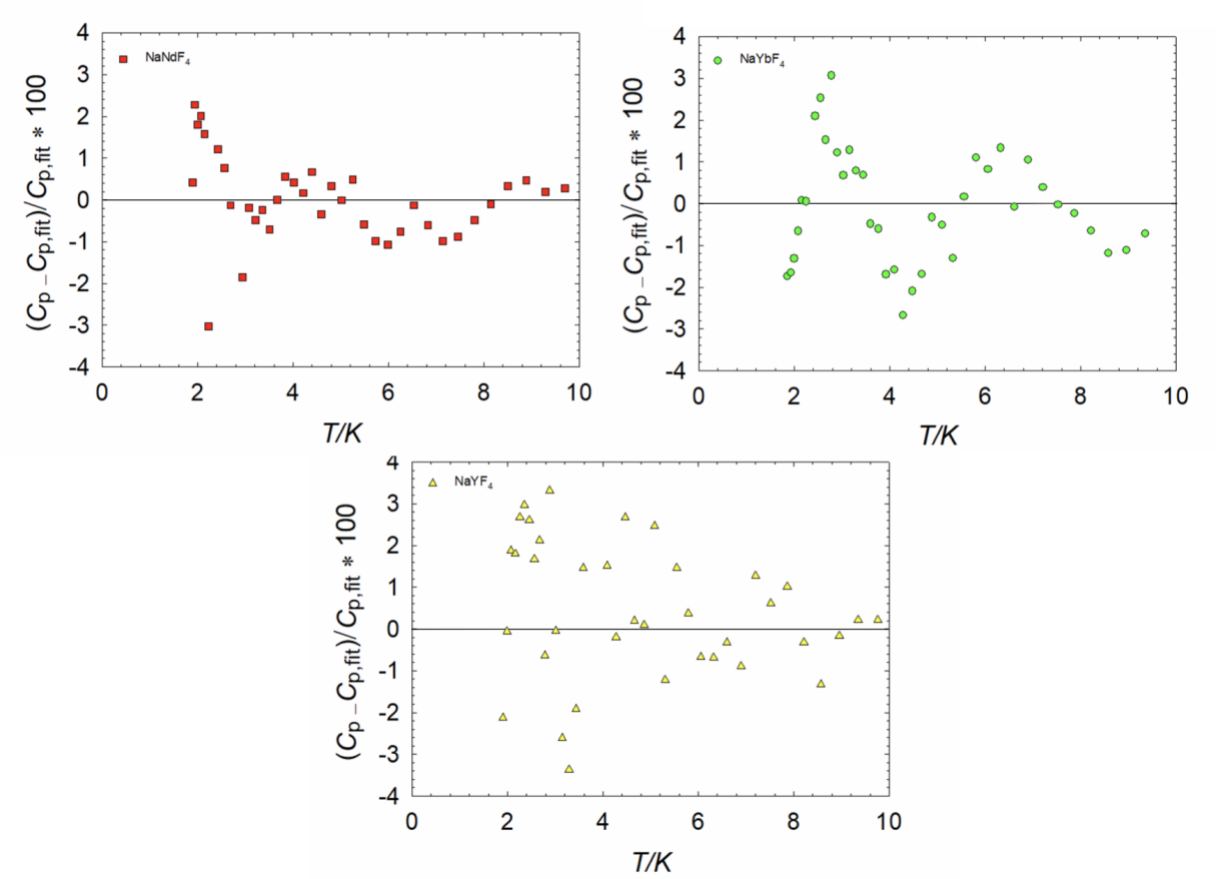

Figure 4. Deviation plots for low temperature fits. Deviation from fits stays below 4% and decrease at as temperature increases.

3.3 Middle Temperature Region Curve Fitting

The middle temperature region was fitted with 8th order orthogonal polynomials according to an algorithm developed by the Westrum group [20]. These polynomials do not have a theoretical basis but are used to generate a smooth transition between the neighboring temperature regions. These polynomials are of the form:

$$C_{p.\mathrm{m}} = \sum_{i=0,1,2}^{8} A_i T^i \qquad (3.4)$$

Fitting parameters are included in Table 2 and deviation plots can be found in Figure 5. Fits appear to "wiggle" through the data but deviations remain below 2%.

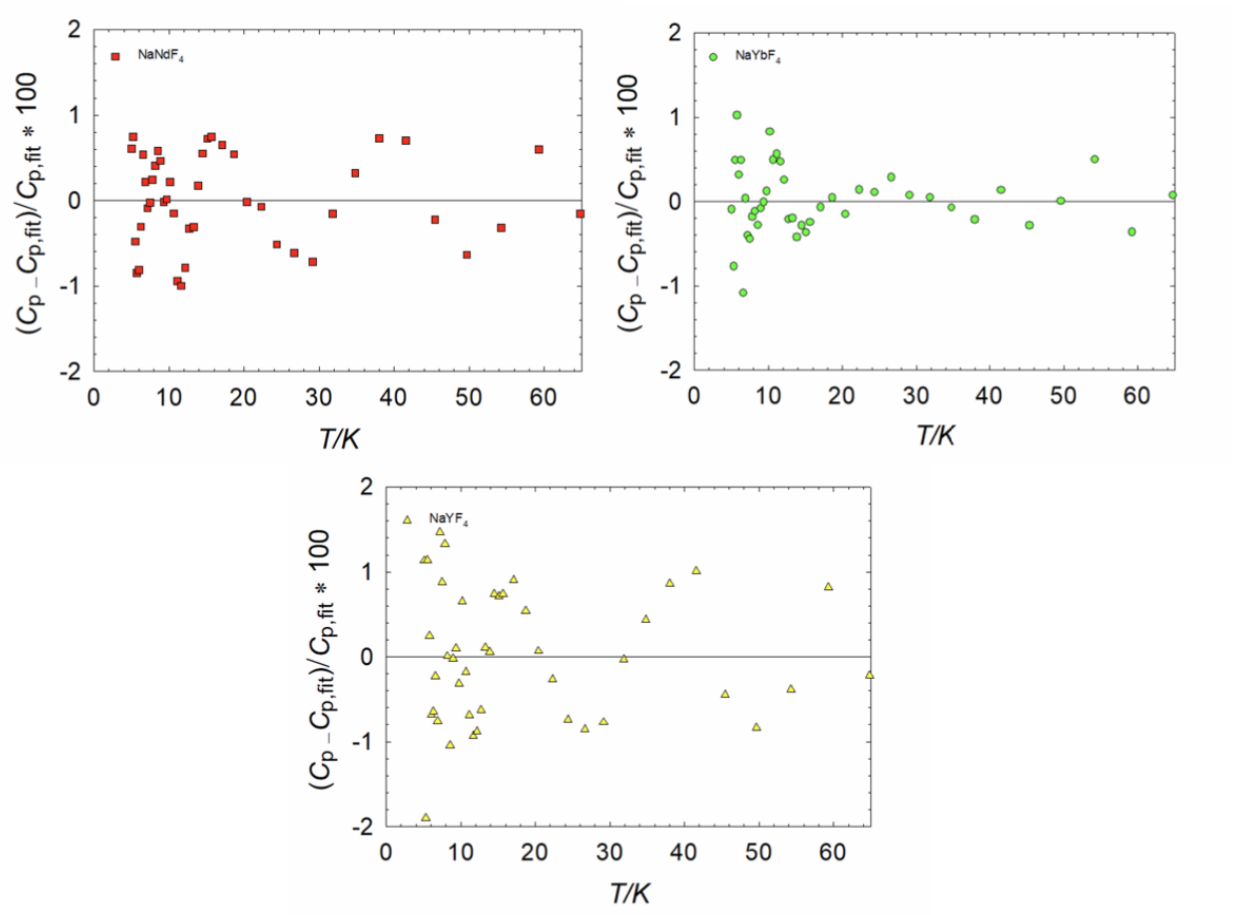

Figure 5. Deviation plots for mid temperature fits. Deviation from fits stays below 2% and show the fit "wiggles" between data.

3.4 High Temperature Region Curve Fitting

The high temperature region was fitted according to the function:

$$C_{p,\mathrm{m}} = m \cdot D(\Theta_D/T) + n_1 \cdot E(\Theta_{E1}/T) + n_2 \cdot E(\Theta_{E2}/T) \tag{3.5}$$

where $D(\Theta_D/T)$ is a Debye function with characteristic temperature Θ_D and $E(\Theta_{E1}/T)$ and $E(\Theta_{E2}/T)$ are Einstein functions with characteristic temperatures Θ_{E1} and Θ_{E2} respectively [11, 13, 21].

$$D(\Theta_D/T) = 9N_a k_B \left(\frac{T}{\Theta_D}\right)^3 \int_0^{\Theta_D/T} \frac{x^4 e^x dx}{(e^x - 1)^2} \tag{3.6}$$

$$E(\Theta_E/T) = 3N_a k_B \left(\frac{\Theta_E}{T}\right)^3 \frac{e^{\Theta_E/T}}{(e^{\Theta_E/T} - 1)^2} \tag{3.7}$$

Here, N_a is the number of atoms and k_B is the Boltzmann constant. Parameters m, n_1, and n_2 represent the number of Debye and Einstein oscillators per mole corresponding to each function [11, 13]. Fitting parameters are included in Table 2 and deviation plots can be found in Figure 6. Deviation plots show deviation remains within 1% and deviation decreases as temperature rises.

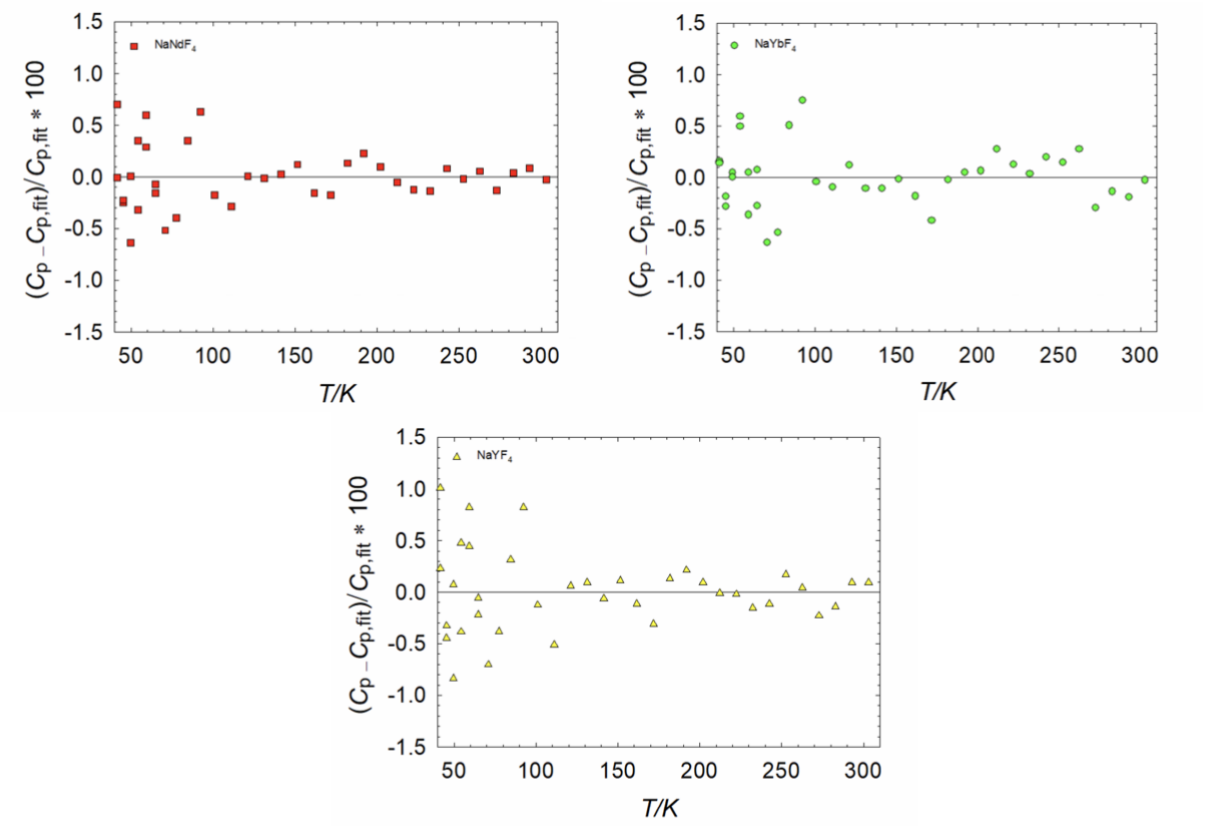

Figure 6. Deviation plots for high temperature fits. Deviation from fits stays below 1% and decreases as temperature increases.

Table 2. Parameters for low T (T < 10 K), mid T (5 K < T < 65 K), and high T (T > 40 K) fits of heat capacity data (in J· K^{-1}· mol^{-1}) for $NaNdF_4$, $NaYbF_4$, and $NaYF_4$.

	Parameter	$NaNdF_4$	$NaYbF_4$	$NaYF_4$
Low T Fits	B_1 / J·K^{-2}·mol^{-1}	$1.5756\cdot10^{-3}$	$3.3070\cdot10^{-3}$	$1.2169\cdot10^{-3}$
	B_3 / J·K^{-4}·mol^{-1}	$2.2519\cdot10^{-4}$	$1.8571\cdot10^{-4}$	$9.1362\cdot10^{-5}$
	B_5 / J·K^{-6}·mol^{-1}	$6.9883\cdot10^{-8}$	$9.9030\cdot10^{-6}$	$6.1490\cdot10^{-7}$
	B_7 / J·K^{-8}·mol^{-1}	$3.1397\cdot10^{-9}$	$-5.7549\cdot10^{-8}$	$-1.4267\cdot10^{-9}$
	a' / K	−0.53300	0.25685	−0.067924
	P / K	0.07700	0.12656	0.0
	%RMS	1.61	1.31	2.10
	Range / K	1.81−8.87	1.86−7.83	1.82−6.13
Mid T Fits	A_0 / J·K^{-1}·mol^{-1}	0.45803	0.38383	0.084868
	A_1 / J·K^{-2}·mol^{-1}	−0.14511	−0.16195	−0.053715
	A_2 / J·K^{-3}·mol^{-1}	0.023696	0.021188	0.014511
	A_3 / J·K^{-4}·mol^{-1}	$-2.3515\cdot10^{-3}$	$-7.9471\cdot10^{-5}$	$-1.9162\cdot10^{-3}$
	A_4 / J·K^{-5}·mol^{-1}	$1.8677\cdot10^{-4}$	$-2.8961\cdot10^{-5}$	$1.5579\cdot10^{-4}$
	A_5 / J·K^{-6}·mol^{-1}	$-7.2002\cdot10^{-6}$	$1.7328\cdot10^{-6}$	$-6.0022\cdot10^{-6}$
	A_6 / J·K^{-7}·mol^{-1}	$1.4698\cdot10^{-7}$	$-4.3900\cdot10^{-8}$	$1.2260\cdot10^{-7}$
	A_7 / J·K^{-8}·mol^{-1}	$-1.5322\cdot10^{-9}$	$5.2066\cdot10^{-10}$	$-1.2799\cdot10^{-9}$
	A_8 / J·K^{-9}·mol^{-1}	$6.4092\cdot10^{-12}$	$-2.3705\cdot10^{-12}$	$5.3624\cdot10^{-12}$
	%RMS	0.53	0.39	0.76
	Range / K	8.87−45.58	7.83−41.23	6.13−44.98
High T Fits	m / mol	5.1534	1.4418	1.7167
	Θ_D / K	430.66	187.52	254.93
	n_1 / mol	0.74740	3.2314	3.6626
	$\Theta_{E,1}$ / K	131.18	333.69	399.25
	n_2 / mol	0.66221	1.6908	1.2503
	$\Theta_{E,2}$ / K	1016.1	625.41	865.14
	%RMS	0.22	0.29	0.29
	Range / K	45.58−303.07	41.23−302.97	44.98−303.06

3.5 Low Temperature Upturns

A low temperature upturn in heat capacity is generally due to the high temperature tails of one or more Schottky anomalies [11]. We attribute the presence of low temperature Schottky anomalies in these samples to spin ordering in nuclei with non-zero spin. A Schottky anomaly occurs in a two-level or multi-level system when the system experiences a substantial change in state occupation as the temperature approaches the energy gap (reduced with the Boltzmann constant) [11, 13]. At temperatures less than the energy gap, the distribution of occupied energy levels heavily favors the ground state; as the temperature approaches the energy gap, the system shifts to a more even distribution. This localized transition between states appears as a peak/upturn in the heat capacity.

Nuclei with nonzero spin are known to exhibit anomalies in low temperature heat capacity data [18, 22-26]. These nuclei exhibit hyperfine structure and, if quadrupolar ($I > \frac{1}{2}$), experience additional interactions with the crystal field gradient [18]. Neodymium and Ytterbium each have two isotopes with nonzero nuclear spin: ^{143}Nd & ^{145}Nd and ^{171}Yb & ^{173}Yb. The only naturally occurring isotope of Yttrium, ^{89}Y, has non-zero spin [27].

The low temperature heat capacity data was originally fitted with a full Schottky function; however, high temperature approximations to a Schottky function were more straightforward, especially when extracting hyperfine field values. A linear term was required when fitting without the full Schottky function. The small magnitude of each linear term suggests that lattice vacancies/impurities were small enough to be masked by the full Schottky function. We therefore believe that the full Schottky function was not as reliable.

3.6 Hyperfine Field Calculations

Using the fitting constant *a'*, we arrive at a value for the hyperfine field, H_{eff}, through the expression

$$a' = \mu_I H_{eff}/k_B I \tag{3.8}$$

where, for each isotope with non-zero spin, μ_I is the nuclear magnetic moment, I is the nuclear spin, and k_B is the Boltzmann constant [18]. The calculated magnetic fields, H_{eff}, are 8330 T for $NaNdF_4$, 3588 T for $NaYbF_4$, and 676 T for $NaYF_4$. The largest upturn was found in $NaNdF_4$ which also had the largest calculated hyperfine field value. We attribute this to notable isotopes of Nd having higher spins and larger magnetic moments than other samples. In addition, both relevant isotopes of Nd experience quadrupolar interactions.

3.7 Conclusions

We measured the heat capacity of three sodium rare earth ternary fluorides, $NaNdF_4$, $NaYbF_4$, and $NaYF_4$. These materials have upturns in their heat capacity indicative of the ordering of nuclear spin states below 6 K. We approximated hyperfine field values at rare earth nuclei based on fits of the nuclear contribution to the heat capacity. Thermodynamics functions of these data, including $C_{p,\mathrm{m}}$, $\Delta S_{\mathrm{m}}°$, $\Delta H_{\mathrm{m}}°$, and $\Phi_{\mathrm{m}}°$, are reported in the appendix.

Appendix

Table 3. Measured molar heat capacity values at constant pressure for $NaNdF_4$. Measurements were performed using a Quantum Design Physical Properties Measurement System (PPMS) with a standard uncertainty of 2% $C_{p,m}$ below about T = 10 K and 1% $C_{p,m}$ from T = (10 to 300) K. The standard uncertainty in temperature is about 4 mK.

T/K	$C_{p,m}$/J·K^{-1}·mol^{-1}	T/K	$C_{p,m}$/J·K^{-1}·mol^{-1}	T/K	$C_{p,m}$/J·K^{-1}·mol^{-1}
1.8106	0.42989	7.8024	0.16643	77.434	54.044
1.8891	0.43104	8.1451	0.18160	84.595	61.603
1.9357	0.42673	8.5053	0.20021	92.469	69.176
1.9997	0.40849	8.8851	0.22225	101.05	75.976
2.0679	0.39272	9.2820	0.24776	111.16	83.688
2.1435	0.37355	9.6978	0.27955	121.21	90.804
2.2210	0.34043	10.149	0.31929	131.34	96.905
2.3121	0.34977	10.636	0.36590	141.42	102.32
2.4243	0.31561	11.129	0.41714	151.50	107.19
2.5619	0.29093	11.633	0.47882	161.63	111.14
2.6873	0.26950	12.152	0.55120	171.76	114.91
2.8086	0.24225	12.692	0.63641	181.85	118.67
2.9367	0.23333	13.251	0.73126	191.95	121.84
3.0705	0.22267	13.848	0.84711	202.06	124.46
3.2095	0.20852	14.466	0.97859	212.16	126.78
3.3559	0.19641	15.108	1.1271	222.27	128.98
3.5069	0.18405	15.624	1.2549	232.37	131.05
3.6649	0.17481	17.071	1.6588	242.49	133.25
3.8312	0.16610	18.663	2.1831	252.57	134.87
4.0133	0.15678	20.392	2.8336	262.68	136.59
4.2067	0.14832	22.291	3.6696	272.80	137.84
4.3945	0.14253	24.369	4.6887	282.89	139.45
4.5879	0.13567	26.641	5.9506	292.98	140.79
4.7992	0.13193	29.123	7.4746	303.07	141.81
5.0153	0.12797	31.836	9.3624		
5.2495	0.12609	34.804	11.623		
5.4815	0.12348	38.049	14.323		
5.7247	0.12288	41.585	17.471		
5.9829	0.12391	45.453	21.012		
6.2505	0.12679	49.675	25.187		
6.5314	0.13162	54.283	29.978		
6.8272	0.13669	59.323	35.260		
7.1322	0.14359	64.831	40.994		
7.4520	0.15324	70.849	47.173		

Table 4. Measured molar heat capacity values at constant pressure for $NaYbF_4$. Measurements were performed using a Quantum Design Physical Properties Measurement System (PPMS) with a standard uncertainty of 2% $C_{p,m}$ below about T = 10 K and 1% $C_{p,m}$ from T = (10 to 300) K. The standard uncertainty in temperature is about 4 mK.

T/K	$C_{p,m}$/J·K^{-1}·mol^{-1}	T/K	$C_{p,m}$/J·K^{-1}·mol^{-1}	T/K	$C_{p,m}$/J·K^{-1}·mol^{-1}
1.8554	0.090721	7.8705	0.31409	77.344	48.469
1.9264	0.086232	8.2185	0.36004	84.496	55.333
1.9978	0.082363	8.5811	0.41073	92.369	62.184
2.0777	0.078692	8.9623	0.46962	100.94	68.537
2.1587	0.075422	9.3600	0.53488	111.04	75.973
2.2466	0.071694	9.7751	0.60803	121.08	82.959
2.3374	0.080014	10.222	0.69613	131.21	89.012
2.4367	0.066442	10.687	0.78623	141.29	94.660
2.5443	0.063681	11.166	0.88768	151.36	99.851
2.6592	0.060366	11.662	0.99748	161.50	104.33
2.7735	0.059054	12.177	1.1165	171.63	108.27
2.9000	0.056079	12.713	1.2435	181.72	112.48
3.0272	0.054344	13.281	1.3909	191.82	115.98
3.1600	0.053645	13.871	1.5485	201.94	119.10
3.2999	0.052797	14.487	1.7273	212.04	122.17
3.4477	0.052636	15.130	1.9191	222.14	124.53
3.5980	0.052430	15.640	2.0815	232.26	126.74
3.7561	0.053326	17.087	2.5712	242.33	129.05
3.9219	0.054314	18.674	3.1608	252.42	130.90
4.0971	0.056671	20.407	3.8568	262.54	132.83
4.2808	0.059131	22.302	4.7130	272.66	133.68
4.4780	0.063643	24.376	5.7261	282.78	135.36
4.6712	0.068850	26.642	6.9528	292.86	136.62
4.8783	0.076175	29.117	8.3858	302.97	138.09
5.0932	0.083779	31.828	10.105		
5.3206	0.092532	34.784	12.112		
5.5603	0.10559	38.020	14.443		
5.8047	0.12033	41.548	17.193		
6.0617	0.13647	45.407	20.178		
6.3299	0.15677	49.624	23.723		
6.6113	0.17751	54.228	27.863		
6.9059	0.20678	59.257	32.217		
7.2121	0.23695	64.760	37.131		
7.5318	0.27232	70.768	42.483		

Table 5. Measured molar heat capacity values at constant pressure for $NaYF_4$. Measurements were performed using a Quantum Design Physical Properties Measurement System (PPMS) with a standard uncertainty of 2% $C_{p,m}$ below about T = 10 K and 1% $C_{p,m}$ from T = (10 to 300) K. The standard uncertainty in temperature is about 4 mK.

T/K	$C_{p,m}$/J·K^{-1}·mol^{-1}	T/K	$C_{p,m}$/J·K^{-1}·mol^{-1}	T/K	$C_{p,m}$/J·K^{-1}·mol^{-1}
1.8202	$5.3814\cdot10^{-3}$	7.8647	0.070894	77.441	40.379
1.9014	$5.4747\cdot10^{-3}$	8.2102	0.079947	84.603	47.033
1.9862	$5.5712\cdot10^{-3}$	8.5729	0.090611	92.477	54.118
2.0718	$5.6941\cdot10^{-3}$	8.9529	0.10510	101.05	60.659
2.1607	$5.7394\cdot10^{-3}$	9.3497	0.12102	111.17	68.154
2.2550	$5.8752\cdot10^{-3}$	9.7645	0.13885	121.22	75.657
2.3535	$6.0168\cdot10^{-3}$	10.211	0.16252	131.35	82.228
2.4548	$6.1561\cdot10^{-3}$	10.680	0.18718	141.44	88.041
2.5601	$6.2992\cdot10^{-3}$	11.163	0.21609	151.51	93.608
2.6692	$6.5690\cdot10^{-3}$	11.662	0.25003	161.65	98.357
2.7821	$6.6692\cdot10^{-3}$	12.180	0.29015	171.78	102.68
2.8841	$7.2240\cdot10^{-3}$	12.720	0.33743	181.89	107.27
3.0097	$7.3738\cdot10^{-3}$	13.282	0.39429	191.96	111.14
3.1454	$7.6346\cdot10^{-3}$	13.875	0.45783	202.07	114.48
3.2842	$8.0785\cdot10^{-3}$	14.491	0.53505	212.17	117.54
3.4307	$8.7961\cdot10^{-3}$	15.133	0.62032	222.27	120.45
3.5825	$9.7987\cdot10^{-3}$	15.648	0.69528	232.37	122.97
3.7416	0.010017	17.095	0.93781	242.46	125.50
3.9091	0.010820	18.685	1.2528	252.56	128.14
4.0848	0.012612	20.417	1.6567	262.66	130.10
4.2720	0.013628	22.316	2.1746	272.78	131.70
4.4650	0.015454	24.392	2.8203	282.87	133.61
4.6606	0.016636	26.662	3.6303	292.96	135.60
4.8689	0.018436	29.142	4.6313	303.06	137.16
5.0849	0.020993	31.853	5.8888		
5.3106	0.022588	34.819	7.4092		
5.5505	0.026031	38.062	9.2631		
5.7952	0.028904	41.596	11.495		
6.0542	0.032253	45.461	13.983		
6.3222	0.036418	49.683	17.053		
6.6018	0.041385	54.292	20.663		
6.8978	0.046780	59.328	24.765		
7.2036	0.054392	64.835	29.334		
7.5232	0.061629	70.854	34.409		

Table 6. Standard thermodynamic functions of $NaNdF_4$. All calculated thermodynamic values have an estimated standard uncertainty $u = 0.02X$ below 15 K and $u = 0.01X$ from 10 K to 300 K where X is the thermodynamic value.

T/K	$C_{p,m}$/J·K^{-1}·mol^{-1}	$\Delta_{0\,K}^{T}S_m^{o}$/J·K^{-1}·mol^{-1}	$\Delta_{0\,K}^{T}H_m^{o}$/kJ·K^{-1}·mol^{-1}	Φ_m^{o}/J·K^{-1}·mol^{-1}
0	0	0	0	0
1	$1.801\cdot10^{-3}$	$1.651\cdot10^{-3}$	$8.441\cdot10^{-7}$	$8.066\cdot10^{-4}$
2	$4.955\cdot10^{-3}$	$3.752\cdot10^{-3}$	$4.053\cdot10^{-6}$	$1.726\cdot10^{-3}$
3	0.01083	$6.758\cdot10^{-3}$	$1.166\cdot10^{-4}$	$2.871\cdot10^{-3}$
4	0.02084	0.01113	$2.709\cdot10^{-4}$	$4.356\cdot10^{-3}$
5	0.03649	0.01734	$5.522\cdot10^{-4}$	$6.296\cdot10^{-3}$
6	0.05952	0.02590	$1.025\cdot10^{-4}$	$8.814\cdot10^{-3}$
7	0.09203	0.03738	$1.774\cdot10^{-4}$	0.01204
8	0.13678	0.05244	$2.907\cdot10^{-4}$	0.01610
9	0.09334	0.07039	$4.430\cdot10^{-4}$	0.02117
10	0.13193	0.08212	$5.547\cdot10^{-4}$	0.02665
15	0.65053	0.20985	$2.214\cdot10^{-3}$	0.06229
20	2.1440	0.57438	$8.726\cdot10^{-3}$	0.13805
25	4.6913	1.3093	0.02543	0.29208
30	7.9997	2.4477	0.05690	0.55099
35	11.827	3.9626	0.10628	0.92592
40	16.057	5.8139	0.17584	1.4179
45	20.635	7.9662	0.26743	2.0233
50	25.510	10.390	0.38268	2.7366
60	35.876	15.948	0.68910	4.4632
70	46.521	22.279	1.1011	6.5482
80	56.856	29.171	1.6185	8.9405
90	66.495	36.433	2.2359	11.589
100	75.249	43.900	2.9454	14.446
110	83.076	51.446	3.7378	17.466
120	90.016	58.978	4.6040	20.612
130	96.150	66.431	5.5354	23.851
140	101.57	73.759	6.5246	27.155
150	106.38	80.934	7.5649	30.502
160	110.66	87.939	8.6505	33.873
170	114.48	94.765	9.7766	37.255
180	117.91	101.41	10.939	40.636
190	121.00	107.87	12.134	44.005
200	123.79	114.15	13.358	47.356
210	126.33	120.25	14.609	50.682
220	128.64	126.18	15.884	53.980
230	130.75	131.94	17.181	57.245
240	132.69	137.55	18.498	60.475
250	134.46	143.00	19.834	63.667
260	136.10	148.31	21.187	66.821
270	137.61	153.47	22.556	69.935
273.15	138.06	155.07	22.990	70.908
280	139.01	158.50	23.939	73.009
290	140.30	163.41	25.335	76.042
298.15	141.28	167.31	26.483	78.484
300	141.50	168.18	26.745	79.034

Table 7. Standard thermodynamic functions of $NaYbF_4$. All calculated thermodynamic values have an estimated standard uncertainty $u = 0.02X$ below 15 K and $u = 0.01X$ from 10 K to 300 K where X is the thermodynamic value.

T/K	$C_{p,m}$/J·K^{-1}·mol^{-1}	$\Delta_{0\,K}^{T}S_m^{\circ}$/J·K^{-1}·mol^{-1}	$\Delta_{0\,K}^{T}H_m^{\circ}$/kJ·K^{-1}·mol^{-1}	Φ_m°/J·K^{-1}·mol^{-1}
0	0	0	0	0
1	$3.503\cdot10^{-3}$	$3.371\cdot10^{-3}$	$1.702\cdot10^{-6}$	$1.669\cdot10^{-3}$
2	$8.410\cdot10^{-3}$	$7.172\cdot10^{-3}$	$7.461\cdot10^{-6}$	$3.441\cdot10^{-3}$
3	0.01722	0.01206	$1.980\cdot10^{-5}$	$5.457\cdot10^{-3}$
4	0.03434	0.01909	$4.465\cdot10^{-5}$	$7.927\cdot10^{-3}$
5	0.06628	0.02984	$9.341\cdot10^{-5}$	0.01116
6	0.12106	0.04636	$1.848\cdot10^{-4}$	0.01555
7	0.20635	0.07099	$3.457\cdot10^{-4}$	0.02160
8	0.33129	0.10611	$6.101\cdot10^{-4}$	0.02984
9	0.47596	0.15320	$1.011\cdot10^{-3}$	0.04083
10	0.64842	0.21204	$1.571\cdot10^{-3}$	0.05491
15	1.8862	0.68885	$7.659\cdot10^{-3}$	0.17828
20	3.6916	1.4656	0.02137	0.39689
25	6.0431	2.5319	0.04548	0.71250
30	8.9254	3.8807	0.08269	1.1243
35	12.274	5.5027	0.13552	1.6307
40	15.972	7.3798	0.20601	2.2295
45	19.887	9.4852	0.29558	2.9168
50	24.032	11.793	0.40528	3.6874
60	32.877	16.947	0.68934	5.4585
70	42.051	22.703	1.0639	7.5046
80	51.105	28.913	1.5299	9.7886
90	59.750	35.436	2.0846	12.274
100	67.837	42.155	2.7231	14.925
110	75.308	48.976	3.4393	17.710
120	82.155	55.827	4.2271	20.601
130	88.397	62.653	5.0804	23.573
140	94.068	69.415	5.9932	26.607
150	99.209	76.083	6.9600	29.683
160	103.86	82.637	7.9757	32.789
170	108.07	89.062	9.0357	35.911
180	111.88	95.349	10.136	39.039
190	115.33	101.49	11.272	42.165
200	118.45	107.49	12.441	45.282
210	121.29	113.34	13.640	48.384
220	123.86	119.04	14.866	51.466
230	126.20	124.60	16.117	54.526
240	128.32	130.01	17.389	57.559
250	130.27	135.29	18.683	60.563
260	132.04	140.44	19.994	63.537
270	133.66	145.45	21.323	66.478
273.15	134.15	147.00	21.745	67.398
280	135.15	150.34	22.667	69.386
290	136.52	155.11	24.025	72.260
298.15	137.55	158.90	25.142	74.577
300	137.78	159.76	25.397	75.099

Table 8. Standard thermodynamic functions of $NaYF_4$. All calculated thermodynamic values have an estimated standard uncertainty $u = 0.02X$ below 15 K and $u = 0.01X$ from 10 K to 300 K where X is the thermodynamic value.

T/K	$C_{p,m}$/J·K^{-1}·mol^{-1}	$\Delta_{0\,K}^{T}S_m^{\circ}$/J·K^{-1}·mol^{-1}	$\Delta_{0\,K}^{T}H_m^{\circ}$/kJ·K^{-1}·mol^{-1}	Φ_m°/J·K^{-1}·mol^{-1}
0	0	0	0	0
1	$1.362\cdot10^{-3}$	$1.304\cdot10^{-3}$	$6.594\cdot10^{-7}$	$6.450\cdot10^{-4}$
2	$3.259\cdot10^{-3}$	$2.784\cdot10^{-3}$	$2.901\cdot10^{-6}$	$1.334\cdot10^{-3}$
3	$6.317\cdot10^{-3}$	$4.633\cdot10^{-3}$	$7.563\cdot10^{-6}$	$2.112\cdot10^{-3}$
4	0.01132	$7.078\cdot10^{-3}$	$1.618\cdot10^{-5}$	$3.033\cdot10^{-3}$
5	0.01928	0.01039	$3.119\cdot10^{-5}$	$4.157\cdot10^{-3}$
6	0.03141	0.01491	$5.613\cdot10^{-5}$	$5.553\cdot10^{-3}$
7	0.04923	0.02102	$9.603\cdot10^{-5}$	$7.305\cdot10^{-3}$
8	0.07375	0.02911	$1.569\cdot10^{-4}$	$9.503\cdot10^{-3}$
9	0.10691	0.03962	$2.464\cdot10^{-4}$	0.01224
10	0.15066	0.05305	$3.742\cdot10^{-4}$	0.01562
15	0.59760	0.18411	$2.064\cdot10^{-3}$	0.04650
20	1.5508	0.47331	$7.204\cdot10^{-3}$	0.11311
25	3.0512	0.97079	0.01849	0.23118
30	5.0407	1.6960	0.03853	0.41169
35	7.4728	2.6501	0.06963	0.66061
40	10.359	3.8311	0.11401	0.98074
45	13.713	5.2405	0.17401	1.3736
50	17.275	6.8670	0.25135	1.8399
60	25.217	10.704	0.46301	2.9871
70	33.893	15.236	0.75815	4.4057
80	42.815	20.344	1.1417	6.0734
90	51.570	25.896	1.6139	7.9640
100	59.890	31.765	2.1716	10.048
110	67.641	37.841	2.8098	12.298
120	74.779	44.037	3.5224	14.684
130	81.313	50.284	4.3033	17.182
140	87.279	56.532	5.1467	19.770
150	92.722	62.742	6.0472	22.428
160	97.692	68.887	6.9996	25.140
170	102.23	74.948	7.9996	27.892
180	106.39	80.911	9.0430	30.672
190	110.19	86.767	10.126	33.471
200	113.68	92.509	11.246	36.280
210	116.89	98.134	12.399	39.092
220	119.84	103.64	13.583	41.901
230	122.55	109.03	14.795	44.703
240	125.06	114.30	16.033	47.493
250	127.37	119.45	17.295	50.269
260	129.50	124.49	18.580	53.027
270	131.47	129.41	19.885	55.765
273.15	132.07	130.94	20.300	56.624
280	133.30	134.23	21.209	58.482
290	135.00	138.94	22.550	61.175
298.15	136.29	142.70	23.656	63.352
300	136.57	143.54	23.908	63.844

Bibliography

1. Gai, S., et al., *Recent Progress in Rare Earth Micro/Nanocrystals: Soft Chemical Synthesis, Luminescent Properties, and Biomedical Applications.* Chemical Reviews, 2014. **114**(4): p. 2343-2389.

2. Li, C. and J. Lin, *Rare earth fluoride nano-/microcrystals: synthesis, surface modification and application.* Journal of Materials Chemistry, 2010. **20**(33): p. 6831-6847.

3. Wang, F., et al., *Simultaneous phase and size control of upconversion nanocrystals through lanthanide doping.* Nature, 2010. **463**(7284): p. 1061-1065.

4. Haas, J.R., E.L. Shock, and D.C. Sassani, *Rare earth elements in hydrothermal systems: Estimates of standard partial molal thermodynamic properties of aqueous complexes of the rare earth elements at high pressures and temperatures.* Geochimica et Cosmochimica Acta, 1995. **59**(21): p. 4329-4350.

5. Zhang, F., et al., *Uniform nanostructured arrays of sodium rare-earth fluorides for highly efficient multicolor upconversion luminescence.* Angewandte Chemie, 2007. **119**(42): p. 8122-8125.

6. Han, S., et al., *Lanthanide-doped inorganic nanoparticles turn molecular triplet excitons bright.* Nature, 2020. **587**(7835): p. 594-599.

7. Sharma, R.K., A.-V. Mudring, and P. Ghosh, *Recent trends in binary and ternary rare-earth fluoride nanophosphors: How structural and physical properties influence optical behavior.* Journal of Luminescence, 2017. **189**: p. 44-63.

8. Yang, S., et al., *Thermochemistry of sodium rare earth ternary fluorides, NaREF4.* Acta Materialia, 2021: p. 117289.

9. Thoma, R.E., H. Insley, and G.M. Hebert, *The Sodium Fluoride-Lanthanide Trifluoride Systems.* Inorganic Chemistry, 1966. **5**(7): p. 1222-1229.

10. Burns, J.H., *Crystal structure of hexagonal sodium neodymium fluoride and related compounds.* Inorganic Chemistry, 1965. **4**(6): p. 881-886.

11. Gopal, E.S.R., *Specific heats at low temperatures*. 1966, New York: Plenum Press. 240.

12. Tamblyn, I. and H.J. Kreuzer, *Thermodynamics*. 2010: World Scientific Publishing Company.

13. Rosen, P.F. and B.F. Woodfield, *Standard methods for heat capacity measurements on a Quantum Design Physical Property Measurement System.* The Journal of Chemical Thermodynamics, 2020. **141**: p. 105974.

14. Kennedy, C.A., et al., *Recommendations for accurate heat capacity measurements using a Quantum Design physical property measurement system.* Cryogenics, 2007. **47**(2): p. 107-112.

15. Shi, Q., et al., *Accurate heat capacity measurements on powdered samples using a Quantum Design physical property measurement system.* The Journal of Chemical Thermodynamics, 2010. **42**(9): p. 1107-1115.

16. Lashley, J.C., et al., *Critical examination of heat capacity measurements made on a Quantum Design physical property measurement system.* Cryogenics, 2003. **43**(6): p. 369-378.

17. Shi, Q., J. Boerio-Goates, and B.F. Woodfield, *An improved technique for accurate heat capacity measurements on powdered samples using a commercial relaxation calorimeter.* The Journal of Chemical Thermodynamics, 2011. **43**(8): p. 1263-1269.

18. Sundström, L.J., *Low temperature heat capacity of the rare earth metals.* Handbook on the Physics and Chemistry of Rare Earths, 1978. **1**: p. 379-410.

19. Schliesser, J.M. and B.F. Woodfield, *Lattice vacancies responsible for the linear dependence of the low-temperature heat capacity of insulating materials.* Physical Review B, 2015. **91**(2).

20. Justice, B.H., *Thermal Data Fitting with Orthogonal Functions and Combined Table Generation. The FITAB Program*. 1969: United States. p. Medium: ED.

21. Kittel, C., *Introduction to solid state physics Eighth edition.* 2021.

22. Heltemes, E. and C. Swenson, *Nuclear contribution to the heat capacity of terbium metal.* The Journal of Chemical Physics, 1961. **35**(4): p. 1264-1265.

23. Neilsen, G., et al., *Quantifying oxygen vacancies in neodymium and samarium doped ceria from heat capacity measurements.* Acta Materialia, 2020. **188**: p. 740-744.

24. Neilsen, G., et al., *Heat capacities and thermodynamic functions of neodymia and samaria doped ceria.* The Journal of Chemical Thermodynamics, 2021. **158**: p. 106454.

25. Ray, M.K., et al., *Origin of cluster spin glass and nuclear Schottky anomaly in Mn50Ni38. 5Sn11. 5 alloy.* EPL (Europhysics Letters), 2015. **109**(4): p. 47006.

26. Woodfield, B.F., M.L. Wilson, and J.M. Byers, *Low-temperature specific heat of La 1− x Sr x MnO 3+ δ.* Physical review letters, 1997. **78**(16): p. 3201.

27. Haynes, W.M., *CRC handbook of chemistry and physics*. 2014: CRC press.

Index

Hyperfine: 6, 19, 20

PPMS: 8-9

Schottky: 12, 14, 19

Upturn: 12-14, 19-20

Thermodynamic Functions: 6-7, 14, 20, 24-26